# Apparent Faster than Light Pulse Propagation

Alejandro Garcia Jr.
University of Texas at Brownsville

## Abstract

Radiation from radio pulses are known to experience dispersion due to free electrons in the ISM: low frequencies are delayed relative to high frequencies. A very different kind of dispersion is theoretically predicted from the 1420.4 MHz resonance of the ISM's neutral hydrogen. This anomalous dispersion makes the group velocity of the pulses larger than the vacuum speed of light. Evidence for such superluminal pulses was first found in observations of PSR B1937+21 two years ago. Another theoretical prediction is that this effect will be different for the left and right polarization modes of the pulses if there is a magnetic field present in the interstellar hydrogen. In this thesis paper, we present follow up observations of this pulsar that confirm the detection and show evidence of birefringence.

# Contents

# 1 Introduction

Radio pulsars are rapidly rotating neutron stars that emit pulses of radio radiation at regular intervals. The apparent pulse period (i.e. the arrival time difference between adjacent pulses) is determined by the rotation period of the star. Hence, the high stability of the observed pulse period is largely due to the rotational stability of these compact stars. The unique properties of radio pulsars allows us to probe various physical and astrophysical phenomenon including test of Newtonian and Einsteinian gravity, ultra-relativistic magneto-hydrodynamics, binary star systems and how they evolve, detection of extrasolar planets, and exotic electromagnetic propagation effects in the interstellar medium (ISM). Soon after the discovery of these objects, it was realized that the ISM will significantly affect the propagation of radio pulses. There have been several different propagation effects studied including: dispersion, absorption, Faraday rotation, scattering, and stimulated emission.

Dispersion of an electromagnetic pulse, or wavepacket, occurs when the pulse is traveling through a medium with a frequency dependent index of refraction. In this case the group velocity of the wavepacket depends on frequency. For the case of the ISM, wavepackets with high frequency content travel faster than wavepackets with low frequency content. For the case of absorption, electrons or other charged particles are present in bound states. Photons in the pulse may excite the bound states to higher energy levels, thereby reducing the total energy present in the pulse as it travels through the ISM. Faraday rotation is a phenomenon whereby the polarization vector of a linearly polarized plane wave rotates about the propagation direction as the waves travels through the ISM. This is typically induced by the presence of an internal magnetic field, which causes a difference in the group veolicty of the left and right circular polarization modes. Scattering effects are created by electron density inhomogenieties present through out the ISM. These density inhomogenieteis refract the parts of the pulse wavefront into and out of the observer's line of sight. Scattering effects manifest themselves as a broadening of pulse profiles and modulation of the pulse power spectrum. Stimulated emission behaves the opposite of absorption; instead of taking a bound state to a higher energy level and "absorbing" the photon energy the bound state is caused to go to a lower energy level resulting in a photon being emitted. Hence, as the pulse travels through the ISM its intensity is seen to increase.

Recently, researchers and students at the University of Texas at Brownsville (UTB) observed the effects of anomalous dispersion in observations of radio pulsar B1937+21, one of the fastest spinning radio pulsars. This effect causes pulses with frequency content near the spin-flip resonance of neutral hydrogen (1420.4 MHz) to appear to travel faster than the speed of light. Unlike recent claims of faster than light neutrino propagation, no laws of physics were harmed by these observations. The apparent faster than light propagation is due to a well known phenomenon known as resonant, or anomalous, dispersion ,where the group velocity goes superluminal near the resonant frequency (Jackson, 1962, section 7.8).

In this thesis we report on a series of observations which confirm the initial discovery originally made by the UTB team. Our recent observations confirm the existence of this phenomenon and may allow us to determine properties of the neutral hydrogen clouds, including the strength of the internal magnetic field. In the next section we review the theory behind anomalous dispersion and estimate the magnitude of the observed effect. The observations and data acquisition process are discussed in section 3. The results of our data analysis will be presented in section 4 followed by our conclusions in section 5.

## 2 Theory

Pulses emitted by a radio pulsar are "broadband," that is to say that they contain a broad range of frequencies. Since the ISM is a dispersive medium, waves with different frequencies will travel at different speeds. The most common dispersive effect observed is known as cold plasma dispersion, where the group velocity increases with increasing frequency, but always remains subluminal. Here we are investigating the dispersive properties of the ISM near the resonant frequency of the electron spin-flip transition in neutral hydrogen. In this case the group velocities become superluminal near the resonant frequency.

In a dispersive medium, the relationship between the wave number, $k$, and frequency, $f$, of the wave determines both the phase and group velocities. This relationship is often refered to as the "dispersion relation." For the case of a cold plasma, the dispersion relation is given by

$$k = \frac{2\pi f}{c}\sqrt{1 - \frac{n_e e^2}{\pi m_e f^2}}, \tag{1}$$

where $m_e$ is the mass of the electron, $e$ is the electron charge, and $n_e$ is the electron number density. From the dispersion relationship, one can calculate the ratio of the speed of light in vacuum, $c$, to the phase velocity of the wave.

This ratio is known as the index of refraction, which is one in vacuum. Using the above equation, one finds that the index of refraction in a cold plasma is given by

$$n(f) = \sqrt{1 - \frac{n_e e^2}{\pi m_e f^2}}. \tag{2}$$

Since the pulses are broadband, they will travel at the "group velocity," which is given by

$$v_g = 2\pi \frac{df}{dk} = c\sqrt{1 - \left(\frac{f_p}{f}\right)^2}. \tag{3}$$

Here, $f_p$ is the plasma frequency, which is equal to $\sqrt{n_e e^2/\pi m_e}$. Using the group velocity, one can calculate the time it takes for a pulse to travel through a region of the ISM. For the case of a spatially uniform medium with an index of refraction $n(f)$, the pulse travel time between the source and the observer is given by:

$$t_d = \frac{D}{v_g} = \frac{D}{c}\frac{1}{2\pi}\frac{dk}{df} = \frac{D}{c}\frac{d}{df}\left(fn(f)\right). \tag{4}$$

For a pulse traveling through a cold plasma with $f >> f_p$, it can be shown that:

$$t_d = \frac{D}{c} + \frac{1}{2}\frac{D}{c}\left(\frac{f_p}{f}\right)^2 \tag{5}$$

where $D$ is the distance traveled by the pulse through the ISM.

Aside from free electrons, the ISM contains clouds of neutral hydrogen. Jenet et al. (2010) showed that the index of refraction within a neutral hydrogen cloud near the spin-flip resonant frequency, $f_0$, is given by:

$$n(f) = 1 + \frac{i\sigma_o c}{4\pi f} w\left(\frac{f - f_c}{\sqrt{2} f_d}\right) \tag{6}$$

where $f_c = f_0(1 - v_c/c)$, $v_c$ is the average velocity of the cloud, $f_d = f_0\sqrt{k_b T/m_h c^2}$ is the thermal frequency width of the cloud, $k_b$ is Boltzmann's constant, $T$ is the kinetic temperature of the cloud, $m_h$ is the mass of a hydrogen atom, and $\sigma_0 = \sqrt{\pi} n_h e^2 s_h/\sqrt{2} m_e f_d c$, where $n_h$ is the number density of hydrogen and $s_h$ is the "oscillator strength". The function $w(z)$ is defined in Abramowitz & Stegun (1970), section 7. The above index of refraction has both a real and imaginary part for frequencies of interest near $f_c$. For the case of a complex index of refraction, the imaginary part determines the optical depth (i.e. the amount of power absorbed by the plasma from the wave), while the real part determines the group velocity and hence the pulse travel time delay across the cloud. From the above index of refraction we find that the optical depth, $\tau(f)$, is given by:

$$\tau(f) = \tau_0 e^{-\frac{(f-f_c)^2}{f_d^2}} \tag{7}$$

where $\tau_0 = \sigma_0 D_c$ and $D_c$ is length scale of the cloud along the line of sight between the observer and the source. By substituting the real part of equation 6 into equation 4 we find the pulse travel time across the cloud of neutral hydrogen is given by:

$$t_d = \frac{D_c}{c} + t_c(f, f_c, f_d, \tau_0), \tag{8}$$

where

$$t_c(f, f_c, f_d, \tau_0) = \tau_0 \left(\frac{f - f_c}{4\pi f_d^2}\right) \mathrm{Im}\left[w\left(\frac{f - f_c}{f_d}\right)\right] - \frac{\tau_0}{2\sqrt{2}\pi^{3/2} f_d}. \tag{9}$$

When $f = f_c$ in equation 9 then the time required for a pulse to travel through the cloud becomes negative. This negative travel time implies that the pulse is traveling faster through the cloud than through vacuum, thus making the pulse appear to be superluminal. Note that the magnitude of the time delay across the neutral hydrogen cloud (i.e the last term on the right-hand side of equation 9) depends on the optical depth and the thermal width of the cloud. The optical depth itself depends on both the temperature and density of the cloud. Hence measuring both the optical depth and the time delay will enable one to independently measure both the cloud temperature and density. This is not possible from measurements of the absorption alone.

For the case where the ISM contains both free electrons and multiple neutral hydrogen clouds along the line of sight, the time delay takes the following form

$$t_d = \frac{D}{c} + \frac{1}{2}\frac{D}{c}\left(\frac{f_p}{f}\right)^2 + \sum_{i=0}^{N_c} t_c(f, f_{ci}, f_{di}, \tau_{0i}), \tag{10}$$

where $N_c$ is the number of clouds along the line of sight, and $f_{ci}$, $f_{di}$, and $\tau_{0i}$ are the values of $f_c$, $f_d$, and $\tau_0$, respectively, for the $i$th cloud.

Dispersion caused by free electrons is observed simultaneously with dispersion caused by the neutral hydrogen clouds. Furthermore, the dispersion from free electrons dominates the time delay. When one measures the pulse time delay as a function of frequency, the slight advancement or delay that is introduced by the H1 clouds will be seen on top of the standard cold plasma dispersion curve. The disperson measure of the cold plasma component can be inferred from the measured time delays at frequencies far from resonance. Given this dispersion measure, the cold plasma time delay may be calcualted for each observed frequency and subtracted from the total time delay. This procedure will allow us to determine the time delays across the neutral hydrogen clouds alone.

# 3 Data Acquisition and Analysis:

## 3.1 Data Acquisition

The data was taken with the National Astronomy and Ionosphere Center's 305 meter Arecibo Telescope located in Puerto Rico. PSR B1937+21 was observed at 12 different epochs in 2011. The details of these observations are summarised in table 3.1. The data was acquired with the Arecibo Signal Processor (ASP) (Demorest, 2007). The signals from each linear polarization of the L-band wide receiver were recorded using ASP. A 4 MHz wide band of each signal centered at 1420.4 MHz was downconverted to baseband, Nyquist sampled, and digitized with 8 bit precision.

Two years ago Jenet et al. (2010) performed the first observations of resonant dispersion with PSR B1937+21 using the L-band wide reciever along with the Wideband Arecibo Pulsar Processors (WAPPs). The observations presented in this work are a significant improvement over those previously reported for several reasons. First, the WAPPs digitize the voltage signal with 3 levels (1.58 bit) as compared to the ASP with 256 levels (8 bit). Second, the WAPPs are an autocorrelation spectrometer and hence the data is divided into frequency bins where the power is then detected and averaged over a certain amount of time. The number of channels and averaging time cannot be changed after the data is recorded. The ASP records Nyquist sampled voltage data, which retains all possible information about the data within the specified bandwidth. This allows for considerable flexibility when analyzing the data.

## 3.2 Preliminary Analysis

After the baseband data has been written to disk by ASP it is necessary to convert the data into a format that can be read by the processing software. The data is converted from a raw data set into a folded data. This is done

| Date | MJD | Duration (s) |
|---|---|---|
| 03-15-2011 | 55635.498912 | 6410.772 |
| 03-16-2011 | 55636.488494 | 6400.192 |
| 03-29-2011 | 55649.4697 | 5505.124 |
| 03-31-2011 | 55651.474479 | 2704.257 |
| 04-01-2011 | 55652.445697 | 6500.819 |
| 04-05-2011 | 55656.435417 | 5618.683 |
| 04-06-2011 | 55657.438282 | 6261.946 |
| 04-11-2011 | 55662.429858 | 6117.353 |
| 04-14-2011 | 55665.4202531 | 7504.226 |
| 04-18-2011 | 55669.393099 | 7469.712 |
| 05-01-2011 | 55682.352774 | 7353.332 |
| 06-01-2011 | 55713.292651 | 5200.420 |

Table 1: *The observations that were used used for the project. The first column consists of the calendar date, the corresponding MJD in the second column, and the duration of the observation is presented in the third column. All of these epochs consisted of a 4 MHz bandwidth and were taken with the L-band wide receiver.*

by using the pulsar's known period and specifying the number of channels to split the bandwidth into. For this work, the folded data set consists of 256 channels and 128 phase bins.

Once the conversion from a baseband data set to a folded data set has taken place, the folded data set can then be dedispersed, which is the removal of dispersion effects caused by free-electrons using a known dispersion measure. Since the main focus is to determine the existence of anomalous dispersion in the folded data set, the 2 polarizations present in the data set can be summed together to obtain the total intensity of the pulses, a process known as "p-scrunching".

Now that the folded data set has been dedispersed and p-scrunched, it is all added together into a single file that has been time scrunched. Time scrunching is simply integrating the entire time together. The action of adding all of the files together is to have the observation of each epoch in a single file to easily compare it to the rest of the epochs. After the data has been added together, the last couple of steps to extract the times of arrival (TOAs) for each frequency can be accomplished.

The first step toward getting the TOAs is to phase align the pulsar between each epoch. The reason for needing to align the phases is because the pulsar will not be exactly in the same phase as it was the last time that it was observed, and the greater the time in between the observations the greater the phase difference there can be. The TOAs for the total intensity of the pulses can then be plotted to determine if they are delayed or advanced around 1420.4 MHz.

### 3.3 Calibration

A propagating plane wave has 2 degrees of freedom, resulting in 2 orthogonal polarizations. In order to study both of these degrees of freedom, one typically uses a set of "crossed-dipole" antennas, where each dipole is sensitive to one particular polarization. Assuming one dipole to be oriented along the "x" direction and the other along the "y" direction, let $E_x$ and $E_y$ be the complex amplitudes of the incident wave's electric field along each of the dipoles, respectively. The incident electric field will induce voltages $v_x$ and $v_y$ in the antenna. It is these voltages that are ultimately recorded by the receivers. The relationship between the measured voltages and the incident electric field components is given by:

$$\begin{pmatrix} v_x \\ v_y \end{pmatrix} = M \begin{pmatrix} E_x \\ E_y \end{pmatrix}, \tag{11}$$

where $M$ is a linear matrix.

If the antenna worked ideally, then $M$ would be equal to:

$$M = \sqrt{G} \begin{pmatrix} 1 & 0 \\ 0 & 1 \end{pmatrix}, \tag{12}$$

where $G$ is the gain of the antenna. In this case:

$$v_x = \sqrt{G} E_x$$
$$v_y = \sqrt{G} E_y.$$

In other words, the voltage along the "x" axis is directly proportional to the incident electric field along that axis, and similarly for the "y" axis.

Unfortunately, no antenna is perfect. Real antennas can introduce various signal distortions including "cross-talk" between the different polarizations as well as differential time delays. In general, these effects may be quantified using more complicated forms of the $M$ matrix. van Straten (2006) recommends a matrix of the following form:

$$M = \sqrt{G} e^{-\gamma - i\phi} \times \begin{pmatrix} e^{2\gamma + i2\phi} \cos(\epsilon_x) & i e^{2\gamma + i2\phi} \sin(\epsilon_x) \\ i \cos(\theta) \sin(\epsilon_y) - \sin(\theta) \cos(\epsilon_y) & \cos(\theta) \cos(\epsilon_y) + i \sin(\theta) \sin(\epsilon_y) \end{pmatrix} \tag{13}$$

where $\theta$ is the angle between the two crossed-dipole antennas minus $\pi/2$, $\phi$ is the instrumentally induced phase difference between the two different polarizations, $\epsilon_{x,y}$ measures the amount of cross-talk between the two polarizations (i.e the amount of $v_x$ induced by $E_y$ and vice-versa) , and $\gamma$ parameterizes the relative gain between the two antennas. For the case of an ideal antenna, all the parameters except for $G$ are equal to zero. In general, these parameters may be frequency dependent. A more detailed explanation on these parameters can be found in van Straten (2004)

One measures the parameters $\gamma$, $\phi$, $\theta$, $\epsilon_x$, and $\epsilon_y$ over the entire bandwidth using a process known as "polarization calibration". During this process, observations of sources with known polarization properties are made. One can compare the known properties to the measured properties and infer the unknown values of the $M$ matrix parameters.

The data is calibrated by using parameter's that model the responses of the instruments, flux density readings, and calibration files taken before or after the pulsar observation. Calibration files are observations of a noise diode coupled to the receptors that represents a 100% linearly polarized reference source.

The flux density of the pulsar has to be normalized by using the flux density of a standard candel, a source with a well known flux density. By normalizing the flux of the pulsar with a known reference source it is possible to get the system noise and flux density as a function of frequency. To do a calibration of the flux, then pointings on- and off-source on the candle are needed. When pointing on-source the telescope is pointing directly at the candle and off-source is when the telescope points at an empty patch of sky.

After the flux density has been normalized, a preliminary polarimetric model can be generated. This preliminary polarimetric model is used to determine the way that the receiver will behave when observing the pulsar pulses. Once the model of how the reciever will respond to the pulses is obtained, then it should be checked to see that the neutral hydrogen spin-flip transition line is not present in the data. If the H1 line is present in the model, then it might be possible that it will not allow for anomalous dispersion to be seen in arrival times of the pulses. This should also be done with the calibrated flux files for the same reasons.

Once the calibration process is complete and the full $M$ matrix is obtained, its inverse may be applied to the measured voltages to determine the components of the incident electric field. These components can then be used to determine the Stoke's parameters independent of any instrumental effects.

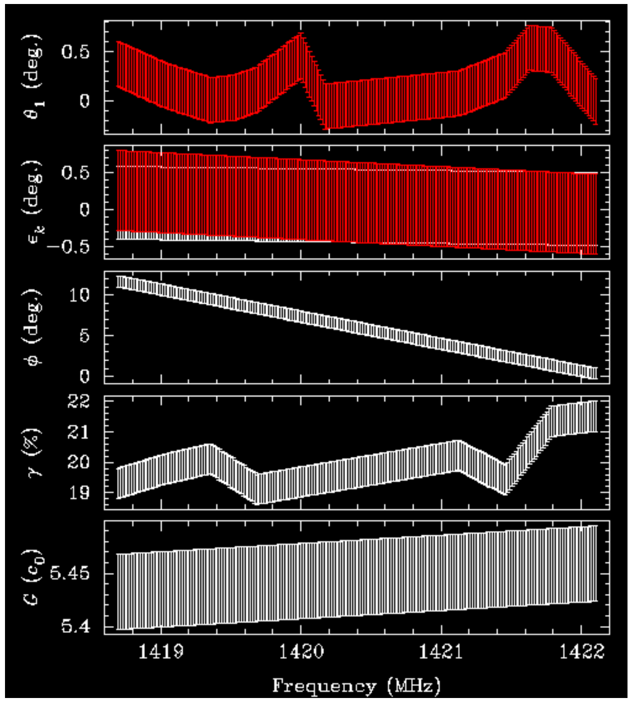


Figure 1: *Plot of the paramters that are fit for during calibration. The first plot is to measure the offset from 90 degrees between the antennas, the second plot is the amount of cross-talk between the two polarizations, the third plot shows the phase difference that is introduce due to the instruments, the fourth plot is the gain of one antenna with respect to the other, and the final plot is the over all gain for the cross-dipole antenna.*

### 3.4 Calibrated Analysis

For the next step, learning more about the neutral hydrogen clouds properties, the polarizations are important; therfore, the procedure changes slightly. The polarizations will not be scrunched together and there will have to be some calibrations done to the pulsar data. The extra steps needed are after the pulsar data has been dedispersed. At this point the steps described in the calibration take place, followed by the same procedure to combine the data for each observation date into a single file.

After the last of the calibration has been completed, the circular polarizations can be extracted from the date. The definition for the circular polarizations was the thumb pointing away from the source and looking at the temperal advance of the Electric field vector. For the left hand circular polarization it is $(I - V)/2$, with the first stokes parameter being $I$ and $V$ being the fourth Stokes parameter. Similarly the right hand circular polarization is obtained from a relationship of $I$ and $V$ , $(I + V)/2$.

Having obtained the circular polarizations of the pulses, they are processed the same way individually. Just like with the preliminary analysis, the phases for each epoch must be aligned together to have a continous model for the pulsar. Following the phase alignment comes the extraction of the TOAs for each frequency in the bandwidth. The TOAs are then plotted in graph to show how the pulsasrs predicted TOAs are compared to the actual TOAs observed. The results from doing the previous procedures can be seen in the following section.

## 4 Results

From the preliminary analysis it is possible to see that the TOAs of the PSR B1937+21 are only affected by anomalouls dispersion caused by the Neutral Hydrogen cloud between the pulsar and the Arecibo Telescope. The reason it can be stated that the anomalous dispersion is affecting the TOAs is because of the advancement only at and around 1420.4 MHz. The effect that anomalous dispersion has on the TOAs can be seen in Figure 1.

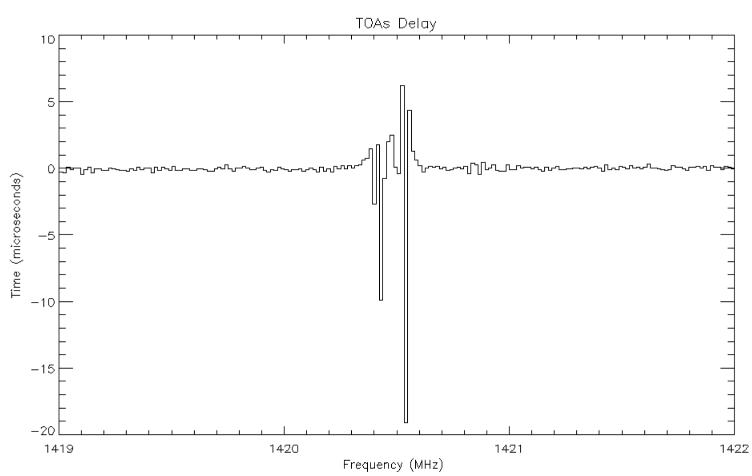


Figure 2: *Delay plot of the TOAs for PSR B1937+21. As can be seen, there is an advancement for the frequencies around 1420.4 MHz. The early arrival times of these frequencies proves the presence of anomalous dispersion.*

From observing the delay plot of the TOAs, one can notice that the TOAs near the resonant frequency of the H1 cloud are arriving almost twenty microseconds earlier than what is expected from the pulsar model. This agrees with previous results presented by Jenet et al. (2010).

After calibrating the pulsar data and extracting the circular polarizations it is possible to plot them. Figure 2 has the plots of the left and right circular polarizations.

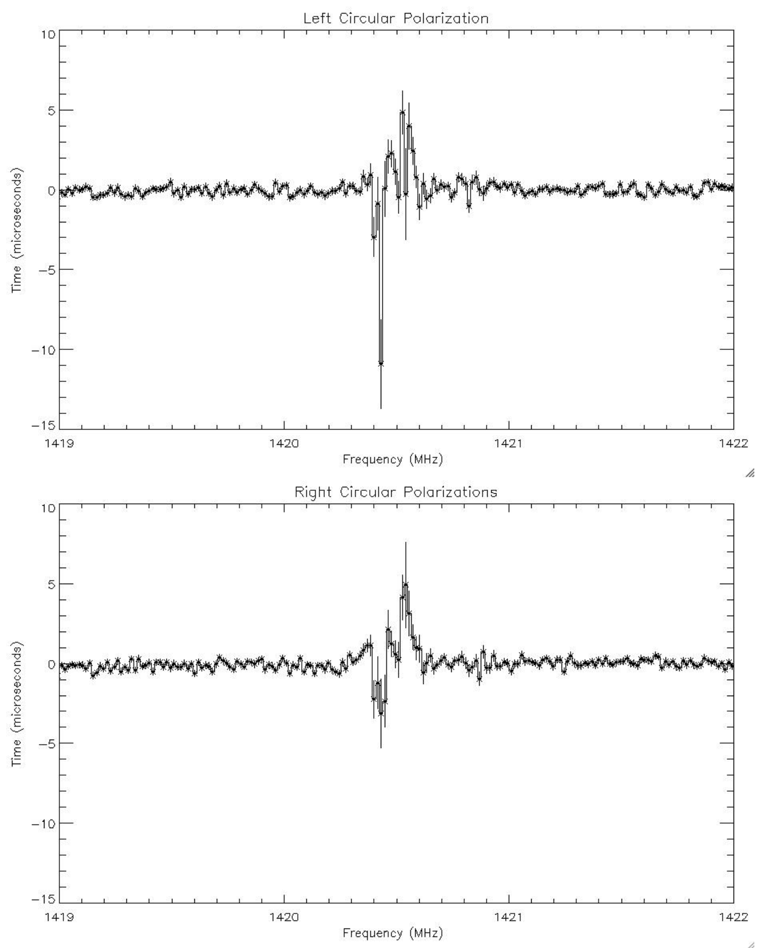


Figure 3: *The plot on the top is the left circular polarization and bottom plot is the right circular polarization. It is obvious that there is a difference between the arrival times of the frequencies for each polarization. These differences imply that the H1 cloud is birefringent.*

As it can be observered from Figure 2, there is a delay in the velocities of the circular polarizations. The left circular polarization seems to be arriving earlier than the right circular polarization by about five microseconds. The reason for the difference in the velocities of the circular polarizations can be caused by the Neutral Hydrogen cloud being "optically active". All molecules are optically active in the presence of magnetic fields, implying that there is a magnetic field present in the H1 cloud the pulses are propagating through.

The error bars in the plots were calculated using the formula

$$error = \frac{1}{SNR}\frac{1}{\sqrt{\sum_{i=0}^{N-1}(\frac{dB}{dt})^2}}. \tag{14}$$

where $B$ is the analytic template that was used as a pulsar model and $SNR$ is the signal to noise ratio of the data set. The $dB/dt$ term is used to model how the pulse profile changes over time.

The $SNR = A/\sigma_N$ where $A$ is the amplitude of the profile and $\sigma_N$ is the rms of the off-pulse noise power. To obtain $A$ the profile can be modeled by the equation:

$$x(t) = AB(t) + n(t) \tag{15}$$

where $B$ is the template, and $n(t)$ is random noise added to the profile. By doing a template matching, one would obtain:

$$\frac{1}{N}\sum_{i=0}^{N-1} B(t_i)x(t_i) = \frac{1}{N}\sum_{i=0}^{N-1} B(t_i)(AP(t_i) + n(t_i)) \tag{16}$$

and simplifying equation 16 while using the assumption that the template is normalized,

$$\frac{1}{N}\sum_{i=0}^{N-1} B(t_i)P(t_i) = 1, \tag{17}$$

then equation 16 becomes

$$\frac{1}{N}\sum_{i=0}^{N-1} AB(t_i)P(t_i) + B(t_i)n(t_i)) = A. \tag{18}$$

The reason that the noise component goes away is because when averaged together the noise will become small enough that it will not have much effect on the rest of the signal.

## 5 Conclusions

From the preliminary analysis it was observed that the pulses with frequencies near 1420.4 MHz were arriving earlier in time as opposed to the rest of the frequencies. The apparent superluminal speeds of the pulses near the spin-flip resonance of neutral hydrogen confirms that there is anomalous dispersion present.

After calibrating the pulsar data it was possible to extract the circular polarizations. From plotting the circular polarizations it was noticed that the left hand circular polarization, as defined from the point of view of the source, had anomalous dispersion present, and the TOAs where arriving earlier in time near 1420.4 MHz. After plotting the right hand circular polarization as well, the anomalous dispersion is also present but the TOAs are only very slightly advanced when compared to the left hand circular polarization. From seeing that the two polarizations were arriving at different times, then the neutral hydrogen cloud must be affecting the propagation of the pulses in another way.

It would be possible to determine the actual orientation and strenghth of the magentic field present in the neutral hydrogen cloud by using the difference in the velocities of the circular polarizations.

## 6 Acknowledgment

I would like to thank the ARCC group for allowing me the chance to participate and providing me with the opportunity to work on a research project. I also thank the Department of Physics and Astronomy at the University of Texas at Brownsville for providing the environment to learn and conduct the research. Another person to thank is Paul Demorest for his help in understanding about the ASP system and help with using psrchive. The person I would like to thank the most would be Dr. Frederick Jenet for all the help with this project and for making all of this possible.

## References

P. B. Demorest. *Measuring the Gravitational Wave Background using Precision Pulsar Timing.* PhD thesis, University of California, Berkeley, August 2007.

J. D Jackson. *Classical Electrodynamics, 2nd Edition.* Wiley, 1962.

F. A. Jenet, D. Fleckenstein, A. Ford, A. Garcia, R. Miller, J. Rivera, and K. Stovall. Apparent faster-than-light pulse propagation in the interstellar space: A new probe of the interstellar medium. *Astrophysical Journal*, 710:1718–1723, February 2010. doi: 10.1088/0004-637X/710/2/1718.

D. R. Lorimer and M. Kramer. *Handbook of Pulsar Astronomy*. Cambridge University Press, 2005.

R. N. Manchester and J. H. Taylor. *Pulsars*. W.H. Freeman and Company, 1980.

W. van Straten. Radio astronomical polarimetry and point-source calibration. *Astrophysical Journal*, 152:129–135, May 2004. doi: 10.1086/383187.

W. van Straten. Radio astronomical polarimetry and high-precision pulsar timing. *Astrophysical Journal*, 642:1004–1011, May 2006. doi: 10.1086/501001.

T. L. Wilso, K. Rohlfs, and S. Hüttemeister. *Tools of Radio Astronomy*. Springer-Verlag, 2009. doi: 10.1007/978-3-540-85122-6.